

Integrable approximation of regular regions with a nonlinear resonance chain

Julius Kullig,^{1,2,3} Clemens Löbner,^{1,2} Normann Mertig,^{1,2,4} Arnd Bäcker,^{1,2} and Roland Ketzmerick^{1,2}

¹*Technische Universität Dresden, Institut für Theoretische Physik and Center for Dynamics, 01062 Dresden, Germany*

²*Max-Planck-Institut für Physik komplexer Systeme, Nöthnitzer Straße 38, 01187 Dresden, Germany*

³*Institut für Theoretische Physik, Universität Magdeburg, Postfach 4120, 39016 Magdeburg, Germany*

⁴*Department of Physics, Tokyo Metropolitan University, Minami-Osawa, Hachioji 192-0397, Japan*

(Dated: November 7, 2014)

Generic Hamiltonian systems have a mixed phase space where regions of regular and chaotic motion coexist. We present a method for constructing an integrable approximation to such regular phase-space regions including a nonlinear resonance chain. This approach generalizes the recently introduced iterative canonical transformation method. In the first step of the method a normal-form Hamiltonian with a resonance chain is adapted such that actions and frequencies match with those of the non-integrable system. In the second step a sequence of canonical transformations is applied to the integrable approximation to match the shape of regular tori. We demonstrate the method for the generic standard map at various parameters.

PACS numbers: 05.45.Mt, 02.30.Ik

I. INTRODUCTION

Hamiltonian systems are an important class of dynamical systems having particular relevance for physical applications, e.g., in celestial mechanics, accelerator dynamics, or mesoscopic and molecular physics. A special case of Hamiltonian systems are integrable systems, where the dynamics is restricted to invariant tori in phase space. The other extreme is given by fully chaotic systems, where the dynamics shows sensitive dependence on the initial conditions and explores the whole phase space.

Generic Hamiltonian systems, however, have a mixed phase space where regions of regular and chaotic motion coexist [1–3]. This is illustrated using the example of the standard map in Fig. 1(a): Here, according to the Kolmogorov–Arnold–Moser (KAM) theorem [4–7], a set of regular tori (lines) forms a regular phase-space region. As predicted by the Poincaré–Birkhoff theorem [8, 9], these tori are interspersed with nonlinear resonance chains leading to a rich self-similar structure. The regular region is embedded in a phase-space region of chaotic motion (dots).

Constructing integrable approximations to regular phase-space regions is helpful or even necessary for many problems, e.g. for toroidal magnetic devices [10], diffusion in random maps [11–13], Arnold diffusion [14, 15], or regular-to-chaotic quantum tunneling [16–19]. Such an integrable Hamiltonian system should mimic the dynamics inside the regular phase-space region as closely as possible. There are situations where it is essential to include a nonlinear resonance chain into the integrable approximation. Here our main motivation is the description of resonance assisted tunneling [20] using complex paths [19] and the fictitious integrable system approach [17] without perturbation theory.

Up to now, integrable approximations can be provided for near-integrable systems, e.g., by using classical

perturbation theory based on Lie-transforms [2, 20–22], normal-form techniques [23–27], or the Campbell–Baker–Hausdorff formula [28–30]. Also for the more challenging case of generic non-integrable systems with a mixed phase space, there are methods available to provide integrable approximations to the regular phase-space region [18, 31]. Particularly flexible is the recently introduced iterative canonical transformation method [31] as it independently accounts for the frequencies and the shape of regular tori and is applicable to higher dimensions. However, in the generic case, none of these methods is so far capable of producing an integrable approximation which includes a nonlinear resonance chain.

In this paper we present a method for constructing an integrable approximation to a regular phase-space region and one nonlinear resonance chain. This is achieved by choosing a normal-form Hamiltonian with a resonance chain [3, 17, 20, 27, 32–34] as the starting point of the iterative canonical transformation method of Ref. [31]. To illustrate the method, we apply it to the generic stan-

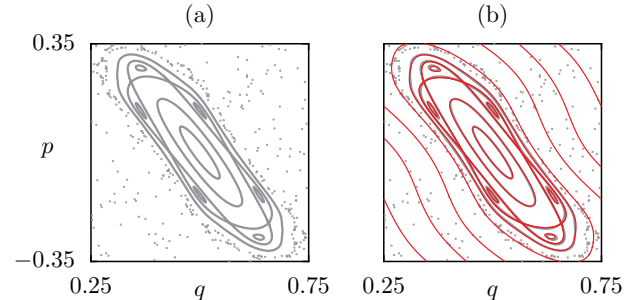


FIG. 1. (color online) (a) Phase space of the standard map, Eq. (3), at $\kappa = 3.4$, with regular orbits (gray lines) and chaotic orbits (gray dots) and (b) its integrable approximation (thin red lines).

dard map, giving, e.g., the integrable approximation of Fig. 1(b).

The paper is organized as follows: In Sec. II we discuss the phase-space structure of a resonance chain using the example of the standard map. In Sec. III we present the method for constructing an integrable approximation to a regular phase-space region and one nonlinear resonance chain. In Sec. IV we apply the method to the standard map. In Sec. V we give a summary and outlook.

II. EXAMPLE SYSTEM WITH A RESONANCE

The construction of integrable approximations described in this paper applies to time-periodically driven Hamiltonian systems with one degree of freedom. These systems obey Hamilton's equations of motion,

$$\dot{q} = \frac{\partial H(q, p, \tilde{t})}{\partial p}, \quad (1a)$$

$$\dot{p} = -\frac{\partial H(q, p, \tilde{t})}{\partial q}, \quad (1b)$$

for position q and momentum p . Considering the corresponding trajectories stroboscopically at times $\tilde{t} = tT$ with $t \in \mathbb{Z}$, that are multiples of the external driving period T , gives a symplectic map U ,

$$(q_{t+1}, p_{t+1}) = U(q_t, p_t), \quad (2)$$

for the evolution of the point (q_t, p_t) to (q_{t+1}, p_{t+1}) in phase space.

The paradigmatic example of such a system is the standard map [3]

$$q_{t+1} = q_t + p_t, \quad (3a)$$

$$p_{t+1} = p_t + \frac{\kappa}{2\pi} \sin[2\pi(q_t + p_t)], \quad (3b)$$

which we consider for $(q, p) \in [0, 1] \times [-0.5, 0.5]$ with periodic boundary conditions. In this paper we focus on $\kappa = 3.4$. Here the standard map has an elliptic fixed point at $(q^*, p^*) = (0.5, 0)$ which is surrounded by a large regular phase-space region embedded in a chaotic phase-space region, see Fig. 2.

According to the KAM theorem [4–7], the regular region is composed of invariant 1D tori, along which the iterated points rotate with a sufficiently irrational frequency ω . Following from the Poincaré–Birkhoff theorem [8, 9], these irrational tori are interspersed by nonlinear $r:s$ resonance chains [2, 3] with rational frequencies

$$\Omega_{r:s} = 2\pi \frac{s}{r}. \quad (4)$$

E.g. for $\kappa = 3.4$, the dominant $r:s = 6:2$ resonance has $r = 6$ resonance regions, see Fig. 2. Here s denotes the number of resonance regions that are surpassed in one iteration step of U . Thus after r periods of the external driving one has s rotations around the elliptic fixed

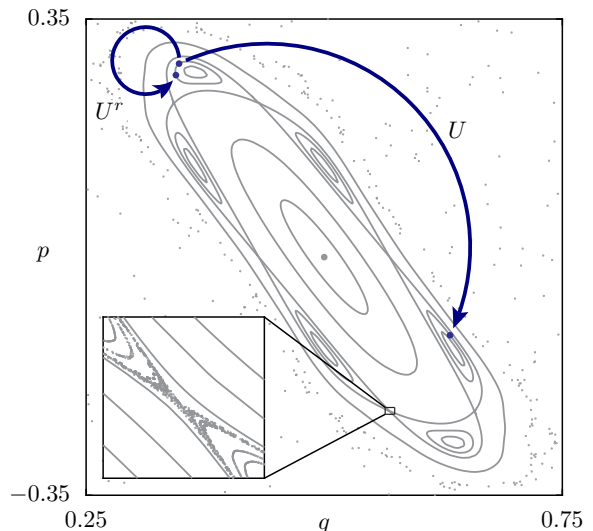


FIG. 2. (color online) Phase space of the standard map, Eq. (3), at $\kappa = 3.4$ with a chaotic orbit (gray dots), regular tori (gray lines) including the dominant 6:2 resonance chain and a chaotic layer (inset). The arrows indicate one iteration step when applying the maps U and U^r .

point (q^*, p^*) . Note that this 6:2 resonance is composed of $s = 2$ disconnected groups of $\frac{r}{s} = 3$ resonance regions. As the rational numbers are dense within the real numbers, there are infinitely many nonlinear resonance chains within the regular region, where the dominant one typically has the lowest order r . Each resonance chain is surrounded by a thin chaotic layer, see the inset in Fig. 2. It is important to note that applying the r -times iterated map U^r gives the same phase-space structure as U , however each resonance region is mapped onto itself, see Fig. 2.

III. ITERATIVE CANONICAL TRANSFORMATION METHOD WITH A RESONANCE

In this section we demonstrate how a regular phase-space region of a mixed system and one considered nonlinear resonance chain can be approximated by an integrable Hamiltonian $H_{r:s}(q, p)$. More specifically, $H_{r:s}(q, p)$ is constructed such that the final point of a time-evolution over the time span $\Delta t = r$ is close to $U^r(q, p)$, if the initial point (q, p) is chosen from the regular region. The reason for using the resonance order r as the time span Δt instead of considering $\Delta t = 1$ is indicated in Fig. 2: Here the r resonance regions are connected by the dynamics of U , a property that cannot be modeled by a time-independent integrable approximation. We consider the r -fold map U^r instead, where each resonance region is mapped onto itself.

In order to find $H_{r:s}(q, p)$, we generalize the iterative

canonical transformation method of Ref. [31] to include the considered nonlinear resonance chain. The iterative canonical transformation method is based on the idea, that the tori of the regular region and their dynamics can be decomposed into the properties (i) action and frequency as well as (ii) shape. Accordingly, an integrable approximation is constructed in two steps: (i) Find an integrable approximation with matching frequencies and actions. (ii) Transform this integrable approximation to match the shape of the tori in phase space using iterative canonical transformations.

To include a resonance chain into the integrable approximation, step (i) is extended to normal-form Hamiltonians [3, 17, 20, 27, 32–34], as discussed in Sec. III A. This is followed by a presentation of step (ii) in Sec. III B. The specific implementation of the iterative canonical transformation method with a resonance for the standard map is demonstrated in Sec. IV.

A. Action and frequency approximation

We now describe the first step of constructing an integrable approximation to a regular phase-space region of U^r and the considered nonlinear resonance chain. This step requires to extract information about the actions and frequencies of motion along tori in the regular phase-space region. This information is then condensed into an integrable approximation.

1. Extracting actions and frequencies of U^r

In order to compute actions and frequencies of U^r , we compute the orbit

$$\bar{\mathbf{x}}_{\ell r}^\tau = (U^r)^\ell(\bar{q}_0^\tau, \bar{p}_0^\tau), \quad (5)$$

with initial conditions $(\bar{q}_0^\tau, \bar{p}_0^\tau)$ for $\ell = 1, \dots, \ell_{\max}$ iterations of U^r . These orbits lie on a set of tori labeled by τ in the regular region, including tori of the resonance regions. Their action \bar{J}_τ can be evaluated according to the general formula

$$J = \frac{1}{2\pi} \oint_{\text{torus}} p \, dq. \quad (6)$$

Their frequency $\bar{\omega}_\tau = \hat{\omega}/r \in [-\frac{\pi}{r}, \frac{\pi}{r}]$ can be determined from the frequency $\hat{\omega}$ of the orbit $\hat{\mathbf{x}}_\ell^\tau = \bar{\mathbf{x}}_{\ell r}^\tau$. Thus the orbit $\bar{\mathbf{x}}_{\ell r}^\tau$ is described by the Fourier series $\bar{\mathbf{x}}_{\ell r}^\tau = \sum_{k \in \mathbb{Z}} \mathbf{c}_k^\tau \exp(i\bar{\omega}_\tau \ell r k)$. Note that this definition of $\bar{\omega}_\tau$ based on U^r is equivalent to the definition of Ref. [17] where the frequencies of U are shifted by $\Omega_{r:s}$ into the co-rotating frame of the $r:s$ resonance. Finally this leads to the dataset of actions and frequencies

$$(\bar{J}_\tau, \bar{\omega}_\tau) \quad (7)$$

of the regular region of U^r . Note that all quantities related to U^r are marked by an overbar to clearly distinguish them from those quantities related to the integrable approximation.

2. Integrable approximation

Based on the determined actions and frequencies we now introduce an integrable approximation. Following the idea of normal forms [3, 17, 20, 27, 32–34], we choose as an ansatz the Hamiltonian

$$\mathcal{H}_{r:s}(\theta, I) = \mathcal{H}_0(I) + \mathcal{V}(I) \cos(r\theta), \quad (8)$$

where r is the order of the resonance. The phase space of this Hamiltonian consists of three integrable parts, see Fig. 3(a), which correspond to the regular region of U^r with the considered resonance chain, see Fig. 3(b). The ansatz for $\mathcal{H}_{r:s}(\theta, I)$ contains two arbitrary functions $\mathcal{H}_0(I)$ and $\mathcal{V}(I)$. They need to be determined according to the following criterion: For every torus of the map U^r with action \bar{J}_τ and frequency $\bar{\omega}_\tau$, there should (i) exist a torus of $\mathcal{H}_{r:s}(\theta, I)$ with the same action $J = \bar{J}_\tau$ having (ii) a similar frequency $\omega(J = \bar{J}_\tau) \approx \bar{\omega}_\tau$. Here $\omega(J)$ is the frequency function induced by the Hamiltonian $\mathcal{H}_{r:s}(\theta, I)$ in the corresponding parts of phase space.

To achieve (i), $\mathcal{H}_0(I)$ and $\mathcal{V}(I)$ are chosen such that the total area $A_{r:s}$ of the resonance regions and the area A_1 below the resonance region agree with the corresponding areas of U^r , see Fig. 3,

$$A_{r:s} \approx \bar{A}_{r:s}, \quad (9a)$$

$$A_1 \approx \bar{A}_1. \quad (9b)$$

To achieve (ii), we further choose $\mathcal{H}_0(I)$ and $\mathcal{V}(I)$ such that the distance of corresponding frequencies in U^r and $\mathcal{H}_{r:s}$,

$$\sum_{\tau} |\bar{\omega}_\tau - \omega(\bar{J}_\tau)|^2, \quad (10)$$

is minimized. An explicit determination of $\mathcal{H}_0(I)$ and $\mathcal{V}(I)$ from these conditions in terms of a series expansion is demonstrated in Sec. IV A for the example of the standard map.

B. Shape approximation

We now show how the second step of the iterative canonical transformation method is implemented. For this the normal-form Hamiltonian $\mathcal{H}_{r:s}(\theta, I)$ with adapted frequencies is transformed to the phase-space coordinates (q, p) such that its time-evolution over the time span $\Delta t = r$ closely agrees with U^r in the regular phase-space region. To achieve this the transformed tori of the integrable approximation should match the shape

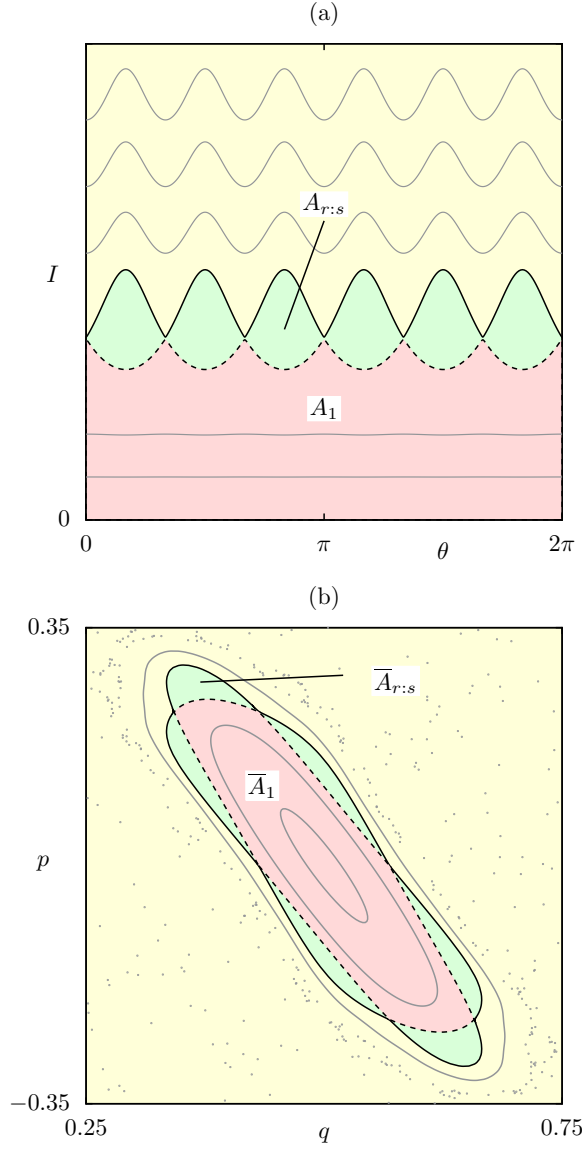


FIG. 3. (color online) (a) Phase space of the normal-form Hamiltonian $\mathcal{H}_{r:s}(\theta, I)$, Eq. (8), with the areas $A_{r:s}$ of the resonance regions and the area A_1 below the resonance regions. (b) The corresponding areas $\bar{A}_{r:s}$ and \bar{A}_1 for the standard map, Eq. (3), at $\kappa = 3.4$.

of the corresponding tori in the regular phase-space region of U^r including the considered nonlinear resonance chain. For this we adapt the iterative canonical transformation method [31] to the case of an additional resonance chain: In Sec. III B 1 we explain how an initial canonical transformation is used to find an initial integrable approximation which roughly resembles the regular phase-space region of the mixed system including the considered resonance chain. In Sec. III B 2 we introduce a family of canonical transformations. In Sec. III B 3 we explain how iterative application of canonical transformations gives an improved integrable approximation.

1. Initial integrable approximation

In order to transform the normal-form Hamiltonian $\mathcal{H}_{r:s}(\theta, I)$ to the phase-space coordinates (q, p) of the regular phase-space region of U^r , we apply an initial canonical transformation

$$T_0 : (\theta, I) \mapsto (q, p). \quad (11)$$

This initial canonical transformation T_0 should map the tori of $\mathcal{H}_{r:s}(\theta, I)$ to the neighborhood of the corresponding tori of U^r . In particular the torus with action $J = 0$ should be mapped onto the fixed point (q^*, p^*) of U^r . This gives the initial integrable approximation

$$H_{r:s}^0(q, p) = \mathcal{H}_{r:s}[T_0^{-1}(q, p)]. \quad (12)$$

It is convenient to choose T_0 in a simple closed form, see Sec. IV B for an example.

2. Family of canonical transformations

In the following we improve the agreement between the tori of the initial integrable approximation $H_{r:s}^0(q, p)$ and those of the regular phase-space region of U^r . To this end we introduce a family of type two generating functions

$$F^{\mathbf{a}}(q, p') = qp' + \sum_{\nu=1}^{\alpha} a_{\nu} G_{\nu}(q, p'), \quad (13)$$

defined by a choice of α parameters $\mathbf{a} = (a_1, a_2, \dots, a_{\alpha}) \in \mathbb{R}^{\alpha}$ and a choice of independent functions G_{ν} . The corresponding canonical transformation

$$T^{\mathbf{a}} : (q, p) \mapsto (q', p') \quad (14)$$

is implicitly defined by the equations

$$q' = \frac{\partial F^{\mathbf{a}}}{\partial p'}(q, p') = q + \sum_{\nu=1}^{\alpha} a_{\nu} \frac{\partial G_{\nu}(q, p')}{\partial p'}, \quad (15a)$$

$$p = \frac{\partial F^{\mathbf{a}}}{\partial q}(q, p') = p' + \sum_{\nu=1}^{\alpha} a_{\nu} \frac{\partial G_{\nu}(q, p')}{\partial q}, \quad (15b)$$

that need to be solved for (q', p') . For sufficiently small \mathbf{a} and bounded C^2 functions G_{ν} this solution globally exists according to Hadamard's global inverse function theorem [35] and represents a near-identity transformation.

3. Iterative improvement

We now use a family of canonical transformations $T^{\mathbf{a}}$ to improve the agreement between the initial integrable approximation $H_{r:s}^0(q, p)$, Eq. (12), and the regular phase-space region of U^r . From a theoretical point of view it is tempting to find a canonical transformation $T^{\mathbf{a}}$ leading to a new Hamiltonian which shows maximal agreement with

the regular phase-space region of U^r . However, finding this transformation, e.g., by making an ansatz for $T^{\mathbf{a}}$ using Fourier basis functions G_ν in Eqs. (13) and (15) with an infinite set of coefficients, is practically impossible. Therefore, we fix the number α of coefficients in our ansatz for the family of canonical transformations $T^{\mathbf{a}}$. Subsequently, we use members from this family to iteratively improve the agreement between the integrable approximation and the regular phase-space region of U^r . This gives a sequence of canonical transformations

$$T_n : (q, p) \mapsto (q', p'), \quad n = 1, 2, \dots, N, \quad (16)$$

with $T_n \in \{T^{\mathbf{a}}\}$ such that the n th integrable approximation

$$H_{r:s}^n(q, p) = H_{r:s}^0 [T_1^{-1} \circ \dots \circ T_n^{-1}(q, p)], \quad (17)$$

agrees more and more with the regular phase-space region of U^r when n is increased.

For this, each canonical transformation has to minimize the distance of points with corresponding action-angle coordinates, $(\vartheta, J) = (\bar{\vartheta}, \bar{J})$, in $H_{r:s}^n$ and U^r , respectively. To achieve this (i) we explain how to obtain the corresponding sample points and (ii) we set up a cost function to minimize their distance.

(i) Using the orbit of Eq. (5), we obtain the sample points $\bar{\mathbf{x}}_{\ell r}^\tau$ of U^r , which correspond to action \bar{J}_τ and angles

$$\bar{\vartheta}_{\ell r}^\tau = \bar{\omega}_\tau \ell r. \quad (18)$$

For the integrable approximation we first define the corresponding sample points of $\mathcal{H}_{r:s}(\theta, I)$,

$$\theta_{\ell r}^\tau = \theta(\vartheta, J) \Big|_{(\vartheta, J) = (\bar{\vartheta}_{\ell r}^\tau, \bar{J}_\tau)}, \quad (19a)$$

$$I_{\ell r}^\tau = I(\vartheta, J) \Big|_{(\vartheta, J) = (\bar{\vartheta}_{\ell r}^\tau, \bar{J}_\tau)}. \quad (19b)$$

Here (ϑ, J) denote the action-angle coordinates of $\mathcal{H}_{r:s}(\theta, I)$ which exist, as $\mathcal{H}_{r:s}(\theta, I)$ is locally integrable. If the used transformation $\theta(\vartheta, J)$, $I(\vartheta, J)$ is known explicitly, as e.g. for the pendulum Hamiltonian [2], an evaluation of Eqs. (19) is straightforward. If this transformation is not known explicitly, which is typically the case, we construct $(\theta_{\ell r}^\tau, I_{\ell r}^\tau)$ using the time evolution with $\mathcal{H}_{r:s}(\theta, I)$. More specifically, we choose $(\theta_0^\tau, I_0^\tau)$ to be the point on the torus of action \bar{J}_τ which is closest to $T_0^{-1}(\bar{\mathbf{x}}_0^\tau)$. We then obtain the points $(\theta_{\ell r}^\tau, I_{\ell r}^\tau)$ from an evolution with $\mathcal{H}_{r:s}(\theta, I)$ up to the time $t = \ell r f$. Here, the factor $f = \bar{\omega}_\tau / \omega(\bar{J}_\tau)$ is of order 1 and ensures that the angle $\vartheta = \omega(\bar{J}_\tau)t = \bar{\omega}_\tau \ell r$ agrees with the corresponding angle $\bar{\vartheta}_{\ell r}^\tau$ of U^r , Eq. (18). Finally this gives the sample points of the n th integrable approximation $H_{r:s}^n(q, p)$,

$$\mathbf{x}_{\ell r}^{\tau, n} = T_n \circ \dots \circ T_1 \circ T_0(\theta_{\ell r}^\tau, I_{\ell r}^\tau), \quad (20)$$

which correspond to the sample points $\bar{\mathbf{x}}_{\ell r}^\tau$ of U^r .

(ii) To minimize the distance between $\bar{\mathbf{x}}_{\ell r}^\tau$ and $\mathbf{x}_{\ell r}^{\tau, n}$ in the $(n+1)$ st iteration step, we apply the canonical transformation $T^{\mathbf{a}}$ and minimize the cost function

$$L(\mathbf{a}) = \frac{1}{\mathcal{N}} \sum_{\tau} \sum_{\ell} [\bar{\mathbf{x}}_{\ell r}^\tau - T^{\mathbf{a}}(\mathbf{x}_{\ell r}^{\tau, n})]^2. \quad (21)$$

Here \mathcal{N} is the total number of sample points. Since $\mathbf{a} = \mathbf{0}$ gives the identity transformation according to Eq. (15), $L(\mathbf{0})$ measures the quality of $H_{r:s}^n$. Thus any choice of \mathbf{a} with $L(\mathbf{a}) < L(\mathbf{0})$ improves $H_{r:s}^n$.

Furthermore, following the strategy of Ref. [31], we determine an optimal parameter \mathbf{a} . To this end we exploit that $H_{r:s}^0(q, p)$ agrees well with the approximated phase-space region already, such that the optimal transformation should be close to the identity transformation, i.e. the sought-for parameter \mathbf{a} is small,

$$|\mathbf{a}| \ll 1. \quad (22)$$

This allows for solving Eq. (15) to linear order, giving a quadratic approximation to the cost function $L(\mathbf{a})$ [31]. From this a good estimate of the optimal parameter \mathbf{a}^* close to the minimum of $L(\mathbf{a})$ is determined. For this parameter \mathbf{a}^* one solves the canonical transformations (15) numerically using Newton's method. If for this parameter \mathbf{a}^* Eq. (15) is not invertible on the relevant domain of phase space, we replace $T^{\mathbf{a}^*}$ by $T^{\eta \mathbf{a}^*}$ using a damping factor $\eta \ll 1$. This is possible as $L(\mathbf{a}^*) < L(\eta \mathbf{a}^*) < L(\mathbf{0})$, but requires to increase the number N of iteration steps.

IV. APPLICATION TO THE STANDARD MAP

In this section we describe how the iterative canonical transformation method with a resonance is implemented for the central regular phase-space region of the standard map. We first consider this map, Eq. (3), for $\kappa = 3.4$, where it has a nonlinear 6:2 resonance, see Fig. 2.

A. Action and frequency approximation

1. Extracting actions and frequencies of U^r

According to Sec. III A 1 we start by determining the actions and frequencies $(\bar{J}_\tau, \bar{\omega}_\tau)$ from the regular phase-space region of the map U^r . For a rough scan of the regular region, we consider a set of points on a line at $\bar{p}_0 = p^*$ with $\bar{q}_0(\lambda) = q^* + \lambda$ using equidistant parameter values $\lambda \in]0, 0.0931]$. To each of these points we apply the map U^r to obtain an orbit and determine its frequency $\bar{\omega}(\lambda)$ [36, 37]. Since frequencies change in a non-smooth way across the infinitely many resonances of the regular region, we focus on so-called noble tori, which are furthest away from these resonances. We determine a set of $\tau_{\max} = 80$ target frequencies $\bar{\omega}_\tau$ from the range of frequencies $\bar{\omega}(\lambda)$ as described in Appendix A. For each

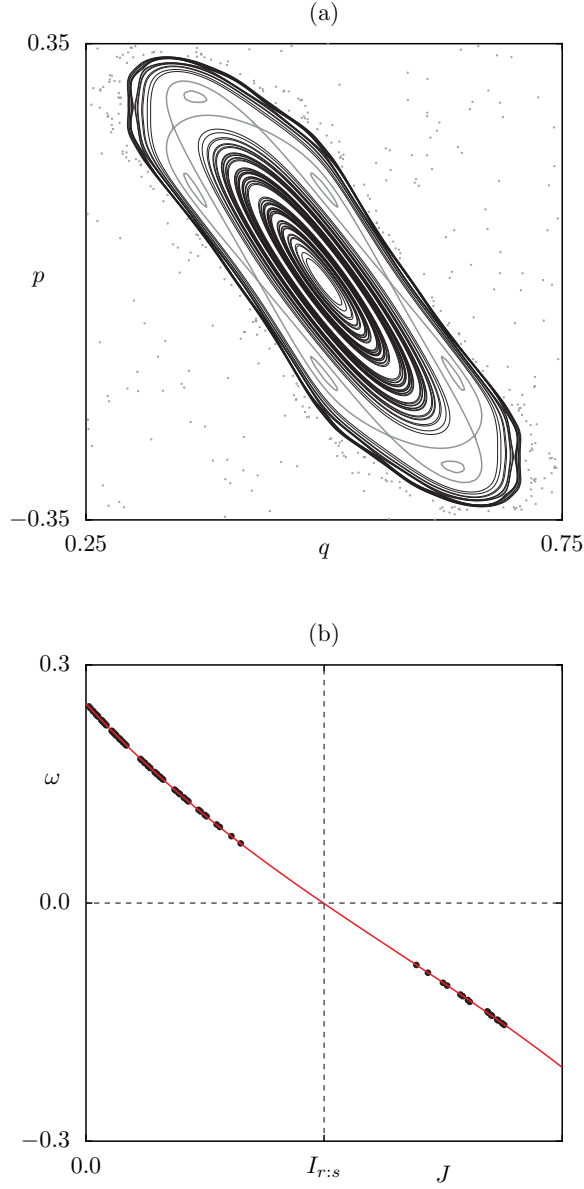


FIG. 4. (color online) (a) Phase space of the standard map, Eq. (3), at $\kappa = 3.4$ (gray lines and dots) with regular orbits $\bar{\mathbf{x}}_{\ell_r}^\tau$ (black) on noble tori. (b) Frequencies $\bar{\omega}_\tau$ of these orbits (black dots) and the fitted function $\mathcal{H}'_0(J)$ (red line).

target frequency $\bar{\omega}_\tau$ we solve $\bar{\omega}(\lambda_\tau) = \bar{\omega}_\tau$ for λ_τ numerically.

This gives a set of initial conditions $(\bar{q}_0^\tau, \bar{p}_0^\tau) = (\bar{q}_0(\lambda_\tau), \bar{p}_0)$ on noble tori τ . From these initial conditions we compute the orbits $\bar{\mathbf{x}}_{\ell_r}^\tau$, Eq. (5), using $\ell_{\max} = 10^4$ iterations of the map U^r , resulting in the black tori shown in Fig. 4(a). We compute their action \bar{J}_τ according to Eq. (6). This gives the dataset of actions and frequencies $(\bar{J}_\tau, \bar{\omega}_\tau)$ which is depicted by the black dots in Fig. 4(b). Note that a similar procedure could be applied to the tori inside the considered resonance chain. However, for convenience we do not use those tori which will turn out

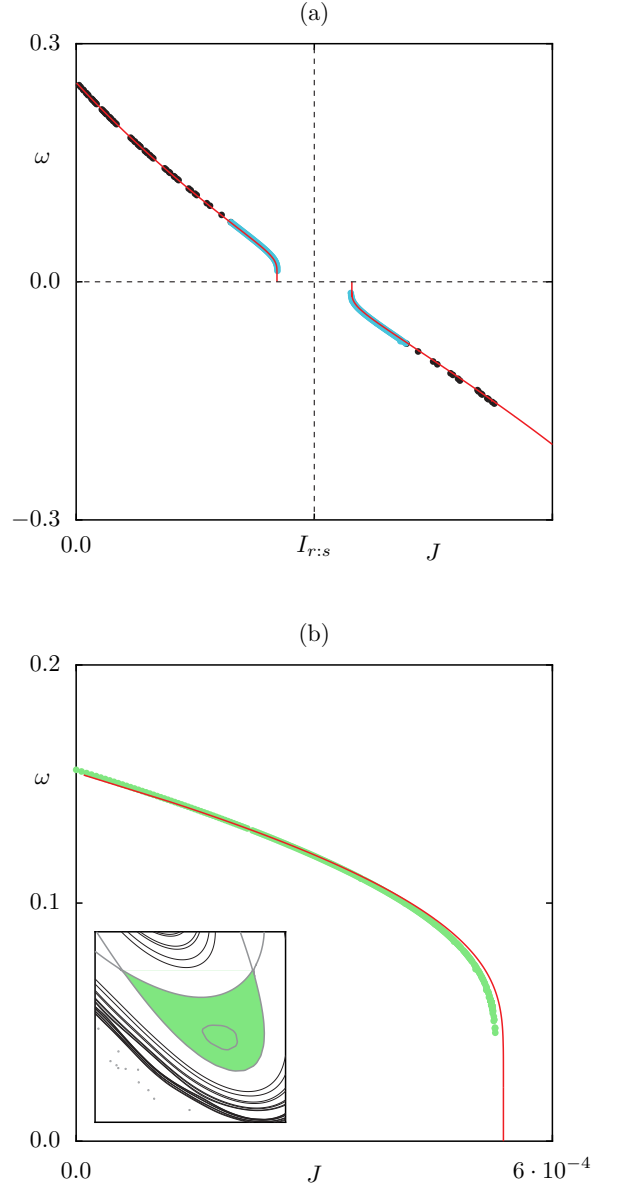


FIG. 5. (color online) Comparison of the frequency function $\omega(J)$ of the determined integrable approximation $\mathcal{H}_{r:s}(\theta, I)$ (red lines) to frequencies of U^r (dots): (a) the frequencies $\bar{\omega}_\tau$ (black dots), frequencies close to the resonance region (light blue dots) and (b) frequencies inside the resonance region (green dots).

to be sufficient.

2. Integrable approximation

As explained in Sec. III A we now require a normal-form Hamiltonian which matches the corresponding actions and frequencies of the standard map U^r by satisfying the area conditions (9) and minimizing Eq. (10). For

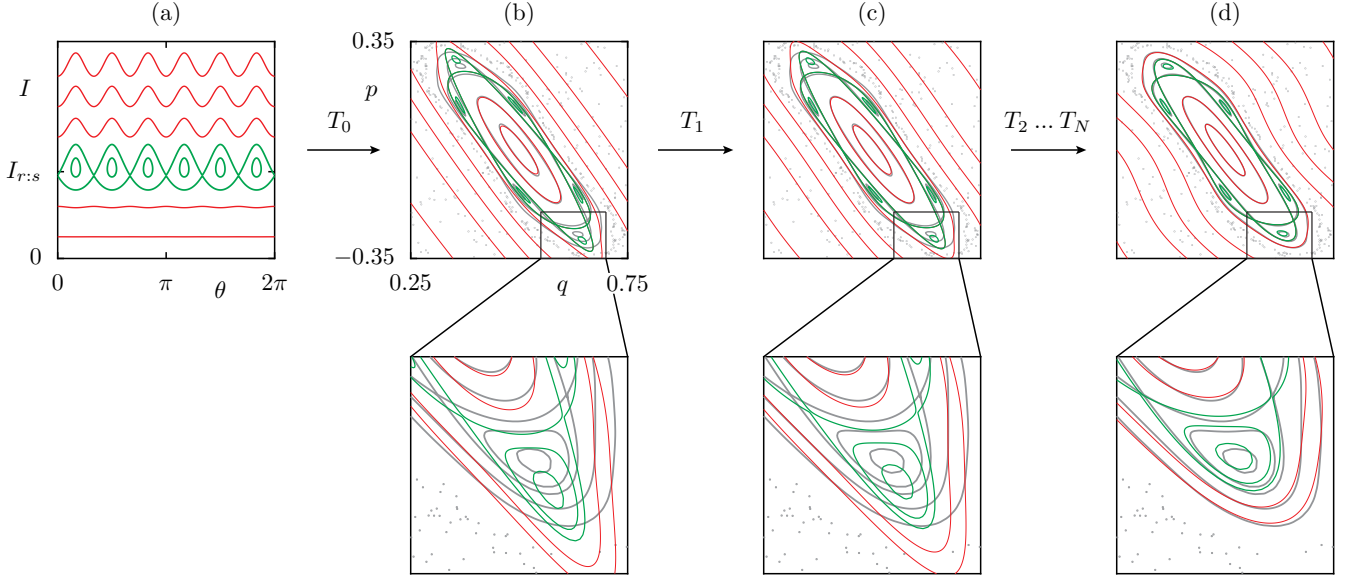


FIG. 6. (color online) (a) Phase space of the normal-form Hamiltonian $\mathcal{H}_{r:s}(\theta, I)$, Eq. (8), with $\mathcal{H}_0(I)$ and $\mathcal{V}(I)$ as determined in Sec. IV A (thin colored lines). (b–d) Phase space of the standard map, Eq. (3), at $\kappa = 3.4$ (light gray lines and dots) and tori (thin colored lines) of the integrable approximations $H_{r:s}^n(q, p)$ obtained from the transformation $T_n \circ \dots \circ T_1 \circ T_0$ (b) $H_{r:s}^0(q, p)$, (c) $H_{r:s}^1(q, p)$, and (d) $H_{r:s}^N(q, p)$, $N = 15$. The magnifications show the improvement of the integrable approximations.

this normal-form Hamiltonian $\mathcal{H}_{r:s}(\theta, I)$, Eq. (8), we use

$$\mathcal{H}_0(I) = \frac{(I - I_{r:s})^2}{2M_{r:s}} + \sum_{k=3}^{\mathcal{K}} h_k (I - I_{r:s})^k, \quad (23)$$

and the lowest order ansatz for a resonance chain encircling a fixed point [17, 27, 34],

$$\mathcal{V}(I) = 2V_{r:s} \left(\frac{I}{I_{r:s}} \right)^{r/2}. \quad (24)$$

In order to determine the unknown parameters $\{I_{r:s}, M_{r:s}, V_{r:s}, h_k\}$ we analyze $\mathcal{H}_{r:s}(\theta, I)$ first close to the resonance and secondly far away from the resonance.

Close to the resonance, the leading order expansion of $\mathcal{H}_{r:s}(\theta, I)$ around $I_{r:s}$ is the pendulum Hamiltonian [20, 32, 33]

$$\mathcal{H}_{r:s}^{\text{pend}}(\theta, I) = \frac{(I - I_{r:s})^2}{2M_{r:s}} + 2V_{r:s} \cos(r\theta). \quad (25)$$

Here $I_{r:s}$ gives the location of the resonance, while $M_{r:s}$ and $V_{r:s}$ control the size $A_{r:s}$ of the resonance and the frequency at the center of the resonance region. We compute these parameters according to [38]

$$I_{r:s} = \frac{1}{2\pi} (\bar{A}_1 + \frac{1}{2} \bar{A}_{r:s}), \quad (26a)$$

$$M_{r:s} = \frac{\mu r^2}{16} \bar{A}_{r:s} \arccos \left(\frac{1}{2} \text{Tr} \bar{\mathcal{M}}_{r:s} \right)^{-1}, \quad (26b)$$

$$V_{r:s} = \frac{\mu}{32r^2} \bar{A}_{r:s} \arccos \left(\frac{1}{2} \text{Tr} \bar{\mathcal{M}}_{r:s} \right). \quad (26c)$$

This accounts for condition (9) by matching the areas $\bar{A}_{r:s}$ and \bar{A}_1 of U^r , see Fig. 3. Furthermore, the frequency at the center of the resonance region enters via the monodromy matrix $\bar{\mathcal{M}}_{r:s}$. Note that these parameters contain the essential information on action and frequency within the resonance regions. Finally, we find for the sign $\mu = -1$, because the frequencies decrease with increasing action, see Fig. 4(b).

We now determine the parameters $\{h_k\}$ which describe the frequency behavior far away from the resonance regions. There the frequency function $\omega(J)$ is approximately described by

$$\omega(J) \approx \mathcal{H}'_0(J) = \frac{J - I_{r:s}}{M_{r:s}} + \sum_{k=3}^{\mathcal{K}} k h_k (J - I_{r:s})^{k-1}, \quad (27)$$

which neglects the resonance as a perturbation. In this approximation, Eq. (10) becomes

$$\sum_{\tau} |\bar{\omega}_{\tau} - \mathcal{H}'_0(\bar{J}_{\tau})|^2, \quad (28)$$

which we minimize to determine $\{h_k\}$. For $\mathcal{K} = 4$ we obtain a satisfactory agreement between the dataset $(\bar{J}_{\tau}, \bar{\omega}_{\tau})$ and the approximate frequency function $\mathcal{H}'_0(J)$, see Fig. 4(b). Note that this comparison is meaningful only far from the resonance, where the approximation (27) is justified.

The determined parameters give the resulting Hamiltonian $\mathcal{H}_{r:s}(\theta, I)$, see Fig. 6(a). For a global comparison, we perform a numerical evaluation of the exact frequency function $\omega(J)$ of $\mathcal{H}_{r:s}(\theta, I)$. We obtain a good agreement

with a mean error of $\Delta\omega = 0.0002$ for the dataset $(\bar{J}_\tau, \bar{\omega}_\tau)$ and also near the resonance (light blue dots in Fig. 5(a)) we have $\Delta\omega < 0.001$. Moreover, even inside the resonance regions where no data of tori has been used for the optimization, but only the parameters of Eqs. (26), the frequency is well approximated, see Fig. 5(b).

B. Shape approximation

We proceed by mapping the integrable approximation obtained in the previous section to the phase space of U^r . As a first step, we choose the initial canonical transformation

$$T_0 : \begin{pmatrix} \theta \\ I \end{pmatrix} \mapsto \begin{pmatrix} q^* \\ p^* \end{pmatrix} + \mathcal{R} \begin{pmatrix} \sqrt{2J} \cos(\theta) \\ -\sqrt{2J} \sin(\theta) \end{pmatrix} \quad (29)$$

with

$$\mathcal{R} = \begin{pmatrix} 1 & 1/2 \\ 0 & 1 \end{pmatrix} \begin{pmatrix} 1/\sqrt{\sigma} & 0 \\ 0 & \sqrt{\sigma} \end{pmatrix}. \quad (30)$$

The parameter σ of T_0 is chosen such that the hyperbolic periodic points of the nonlinear resonance chain along the line $p = 0$ agree both for the standard map and the induced initial integrable approximation $H_{r:s}^0(q, p)$, Eq. (12). The specific choice for T_0 incorporates the symmetries of the standard map into the initial integrable approximation. The result for $\kappa = 3.4$ using $\sigma = 3.96851$ is depicted in Fig. 6(b).

To improve the initial integrable approximation we define the family of canonical transformations $T^{\mathbf{a}}$ using the Fourier ansatz for the generating function

$$\begin{aligned} F^{\mathbf{a}}(q, p') &= qp' \\ &+ \sum_{\nu_1=0}^{\mathcal{N}_q} \sum_{\nu_2=0}^{\mathcal{N}_p} a_{\nu_1 \nu_2}^+ f_{\nu_1}^+ \left(\frac{q - q^*}{\mathcal{L}_q} \right) f_{\nu_2}^+ \left(\frac{p - p^*}{\mathcal{L}_p} \right) \\ &+ \sum_{\nu_1=1}^{\mathcal{N}_q} \sum_{\nu_2=1}^{\mathcal{N}_p} a_{\nu_1 \nu_2}^- f_{\nu_1}^- \left(\frac{q - q^*}{\mathcal{L}_q} \right) f_{\nu_2}^- \left(\frac{p - p^*}{\mathcal{L}_p} \right), \end{aligned} \quad (31)$$

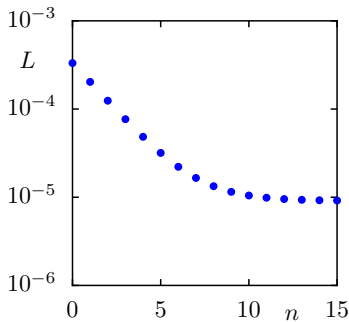


FIG. 7. (color online) Cost function L , Eq. (21), vs. iteration step n .

with basis functions

$$f_\nu^+(x) = \cos(2\pi\nu x), \quad (32a)$$

$$f_\nu^-(x) = \sin(2\pi\nu x). \quad (32b)$$

This ansatz gives canonical transformations, Eq. (14), which preserve the parity of the standard map. Since shifting the generating function by a constant term is irrelevant for the canonical transformation, we set $a_{00}^+ = 0$. Furthermore we choose $\mathcal{L}_q = \mathcal{L}_p = 1.1$ and $\mathcal{N}_q = \mathcal{N}_p = 3$.

In order to set up the cost function $L(\mathbf{a})$, Eq. (21), we compute the sample points $\bar{\mathbf{x}}_{\ell_r}^\tau$ within the regular phase-space region of the standard map, using Eq. (5) with $\ell_{\max} = 10^3$ iterations for the same initial conditions $\bar{\mathbf{x}}_0^\tau$ as in Sec. IV A. Hence, $\bar{\mathbf{x}}_{\ell_r}^\tau$ are points on noble tori of action \bar{J}_τ and frequency $\bar{\omega}_\tau$. We compute the corresponding sample points $\mathbf{x}_{\ell_r}^{\tau,0}$ of $H_{r:s}^0(q, p)$ by numerical integration over times $t = \ell_r \bar{\omega}_\tau / \omega(\bar{J}_\tau)$, as explained in Sec. III B 3. For this we use initial conditions $\mathbf{x}_0^{\tau,0}$ on the line $p = p^*$, $q > q^*$, such that the corresponding tori have action \bar{J}_τ .

Having defined the sample points $\bar{\mathbf{x}}_{\ell_r}^\tau$ and $\mathbf{x}_{\ell_r}^{\tau,0}$, we now minimize the cost function $L(\mathbf{a})$, Eq. (21), according to the procedure described in Sec. III B 3, i.e., we iteratively determine and apply canonical transformations T_n from the family of canonical transformations defined by Eq. (31). Here, we use the damping factor $\eta = 0.25$. Applying $N = 15$ steps of the iterative canonical transformation method, we typically observe a saturation of the cost function, see Fig. 7, giving a sequence of improved integrable approximations $H_{r:s}^n(q, p)$ as shown in Fig. 6. The final integrable approximation $H_{r:s} = H_{r:s}^N$ gives a very good description of the regular region and the 6:2 resonance regions. Even the tori inside the resonance regions which have not yet been included in the cost function, are well approximated.

In Fig. 8 we show integrable approximations for further parameters $\kappa = 2.9, 3.3, 3.5$ of the standard map also including a case with a 10:3 resonance. Here we used the same procedure with parameters $\tau_{\max} = 80$, $\mathcal{K} = 4$, $\mathcal{L}_q = \mathcal{L}_p = 1.1$, $\mathcal{N}_q = \mathcal{N}_p = 3$, $\ell_{\max} = 10^3$, and damping factors $\eta = 0.1, 0.4, 0.25$, respectively. This demonstrates the general applicability of the presented method.

V. SUMMARY AND OUTLOOK

In this paper we present how an integrable approximation can be constructed to the regular phase-space region of a mixed system and one nonlinear resonance chain. In order to achieve this goal we combine the theory of normal-form Hamiltonians with the iterative canonical transformation method. We apply this approach to the generic standard map for various parameter values and find an integrable approximation which closely resembles the dynamics in the regular phase-space region including the considered resonance chain.

One possible generalization of this approach would be to approximate multiple resonance chains. This would

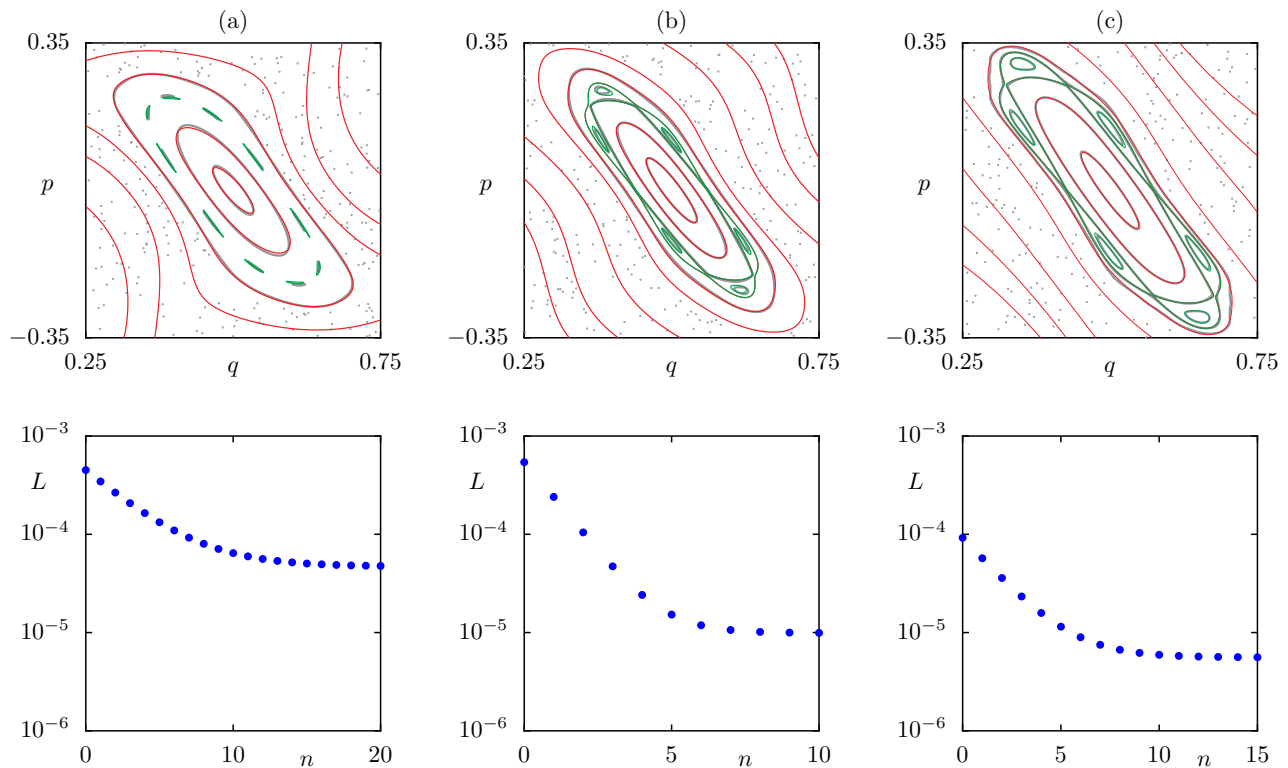


FIG. 8. (color online) Integrable approximations for the standard map, Eq. (3), at different parameters (a) $\kappa = 2.9$, (b) $\kappa = 3.3$, and (c) $\kappa = 3.5$. Top: Phase space of the standard map (light gray lines and dots) and tori of the integrable approximation (thin colored lines). Bottom: Cost function L , Eq. (21), vs. iteration step n .

require normal-form Hamiltonians with more than one nonlinear resonance chain, which is the topic of current research [39]. Another generalization would be the application to systems with a higher-dimensional phase space. Here the main difficulty is to find an integrable normal-form Hamiltonian with tori of appropriate actions and frequencies. On the other hand, the shape approximation using the iterative canonical transformation method should be straightforward.

ACKNOWLEDGMENTS

We thank Jérémy Le Deunff and Peter Schlagheck for stimulating discussions. Furthermore, we acknowledge support by the Deutsche Forschungsgemeinschaft (Germany) within the Forschergruppe 760 *Scattering Systems with Complex Dynamics*. N. M. acknowledges support by JSPS (Japan) grant No. PE 14701. J. K., C. L., and N. M. contributed equally to this work.

Appendix A: Determination of noble frequencies

In this appendix we describe the determination of frequencies $\bar{\omega}_\tau$ of noble tori τ inside the regular region. Ac-

cording to the KAM theorem [4–7] tori persist, for which $\bar{\omega}_\tau/(2\pi)$ is sufficiently irrational, i.e. satisfies a Diophantine condition. This is for example fulfilled for noble numbers whose continued fraction expansion is eventually periodic with 1. Such noble numbers are as far as possible away from rationals in the sense that they are hardest to approximate by rationals [40]. Thus noble tori are particularly suited for the iterative canonical transformation method.

For convenience, we relate the frequencies $\bar{\omega}_\tau$ to numbers $\xi_\tau \in [0, 1[$ by

$$\xi_\tau = \frac{\bar{\omega}_\tau}{2\pi} \mod 1. \quad (\text{A1})$$

We now calculate τ_{\max} noble numbers ξ_τ . This is done by first constructing the Stern–Brocot tree [41–43] of rational numbers and then determining corresponding noble numbers.

1.) To build the Stern–Brocot tree in the interval $[0, 1]$ one starts in the first level with the two fractions $m/n = 0/1$ and $m'/n' = 1/1$. In each iteration for each pair of adjacent fractions m/n and m'/n' we insert the mediant $\zeta = (m + m')/(n + n')$. This leads to the sequence of sets $\{0/1, 1/1\}$, $\{0/1, 1/2, 1/1\}$, $\{0/1, 1/3, 1/2, 2/3, 1/1\}$, Alternatively one could also use the Farey tree [40, 44] which is a subtree of the Stern–Brocot tree.

2.) For each new rational ζ of a level one determines its finite continued fraction expansion

$$\zeta = \zeta_0 + \frac{1}{\zeta_1 + \frac{1}{\zeta_2 + \frac{1}{\ddots + \frac{1}{\zeta_k}}}}, \quad (\text{A2a})$$

$$=: [\zeta_0; \zeta_1, \zeta_2, \dots, \zeta_k]. \quad (\text{A2b})$$

Appending the infinite continued fraction expansion of the golden mean $\sigma = (\sqrt{5} - 1)/2 = [0; 1, 1, 1, \dots]$ at the end of the continued fraction expansion (A2) gives the

noble number

$$\xi = [\zeta_0; \zeta_1, \zeta_2, \dots, \zeta_k, 1, 1, 1, \dots]. \quad (\text{A3})$$

The construction is such that there is precisely one such noble number between each pair of adjacent rationals of a given level of the Stern–Brocot tree.

3.) Each noble number ξ leads to a frequency $\bar{\omega}$ according to Eq. (A1).

4.) The iteration is stopped when τ_{\max} frequencies are found within the range of frequencies $\bar{\omega}(\lambda)$ of the regular region.

-
- [1] L. Markus and K. R. Meyer, no. 144 in Mem. Amer. Math. Soc. (American Mathematical Society, Providence, Rhode Island, 1974).
 - [2] A. J. Lichtenberg and M. A. Lieberman, *Regular and chaotic dynamics* (Springer, New York, 1992), 2nd ed.
 - [3] B. V. Chirikov, Phys. Rep. **52**, 263 (1979).
 - [4] A. N. Kolmogorov, Dokl. Akad. Nauk. SSSR **98**, 527 (1954), english translation in G. Casati and J. Ford, *Stochastic Behavior in Classical and Quantum Hamiltonian Systems*, vol. 93 of *Lect. Notes Phys.* (Springer, Berlin, 1979), 51–56.
 - [5] V. I. Arnold, Russ. Math. Surv. **18**, 9 (1963).
 - [6] V. I. Arnold, Russ. Math. Surv. **18**, 85 (1963).
 - [7] J. Moser, Nachr. Akad. Wiss. Göttingen **1**, 1 (1962).
 - [8] H. Poincaré, Rend. Circ. Mat. Palermo **33**, 375 (1912).
 - [9] G. D. Birkhoff, Trans. Amer. Math. Soc. **14**, 14 (1913).
 - [10] S. R. Hudson and R. L. Dewar, Phys. Lett. A **247**, 246 (1998).
 - [11] A. Bazzani, S. Siboni, G. Turchetti, and S. Vaienti, Phys. Rev. A **46**, 6754 (1992).
 - [12] A. Bazzani, S. Siboni, and G. Turchetti, J. Phys. A **30**, 27 (1997).
 - [13] A. Kruscha, R. Ketzmerick, and H. Kantz, Phys. Rev. E **85**, 066210 (2012).
 - [14] V. I. Arnold, Sov. Math. Dokl. **5**, 581 (1964).
 - [15] P. M. Cincotta, New Astron. Rev. **46**, 13 (2002).
 - [16] A. Bäcker, R. Ketzmerick, S. Löck, and L. Schilling, Phys. Rev. Lett. **100**, 104101 (2008).
 - [17] S. Löck, A. Bäcker, R. Ketzmerick, and P. Schlagheck, Phys. Rev. Lett. **104**, 114101 (2010).
 - [18] A. Bäcker, R. Ketzmerick, and S. Löck, Phys. Rev. E **82**, 056208 (2010).
 - [19] N. Mertig, S. Löck, A. Bäcker, R. Ketzmerick, and A. Shudo, Europhys. Lett. **102**, 10005 (2013).
 - [20] O. Brodier, P. Schlagheck, and D. Ullmo, Ann. Phys. (N.Y.) **300**, 88 (2002).
 - [21] A. Deprit, Celestial Mech. **1**, 12 (1969).
 - [22] J. R. Cary, Phys. Rep. **79**, 129 (1981).
 - [23] G. D. Birkhoff, Acta Math. **50**, 359 (1927).
 - [24] F. G. Gustavson, Astron. J. **71**, 670 (1966).
 - [25] K. R. Meyer, Celestial Mech. **9**, 517 (1974).
 - [26] R. Schubert, H. Waalkens, and S. Wiggins, Phys. Rev. Lett. **96**, 218302 (2006).
 - [27] P. Lebœuf and A. Mouchet, Ann. Phys. (N.Y.) **275**, 54 (1999).
 - [28] R. Scharf, J. Phys. A **21**, 4133 (1988).
 - [29] V. V. Sokolov, Theor. Math. Phys. **67**, 464 (1986).
 - [30] H. Yoshida, Celest. Mech. Dyn. Astr. **56**, 27 (1993).
 - [31] C. Löbner, S. Löck, A. Bäcker, and R. Ketzmerick, Phys. Rev. E **88**, 062901 (2013).
 - [32] A. M. Ozorio de Almeida, *Hamiltonian Systems: Chaos and Quantization* (Cambridge University Press, Cambridge, 1988).
 - [33] O. Brodier, P. Schlagheck, and D. Ullmo, Phys. Rev. Lett. **87**, 064101 (2001).
 - [34] J. Le Deunff, A. Mouchet, and P. Schlagheck, Phys. Rev. E **88**, 042927 (2013).
 - [35] S. G. Krantz and H. R. Parks, *The Implicit Function Theorem: History, Theory, and Applications* (Birkhäuser, Boston, 2002).
 - [36] J. Laskar, C. Froeschlé, and A. Celletti, Physica D **56**, 253 (1992).
 - [37] R. Bartolini, A. Bazzani, M. Giovannozzi, W. Scandale, and E. Todesco, Part. Accel. **52**, 147 (1996).
 - [38] C. Eltschka and P. Schlagheck, Phys. Rev. Lett. **94**, 014101 (2005).
 - [39] J. Le Deunff, A. Mouchet, P. Schlagheck, and A. Shudo (private communication).
 - [40] G. H. Hardy and E. M. Wright, *An Introduction to the Theory of Numbers* (Clarendon Press, Oxford, 1975), 4th ed.
 - [41] M. A. Stern, J. reine angew. Math. **55**, 193 (1858).
 - [42] A. Brocot, Revue Chronométrique **3**, 186 (1860).
 - [43] R. L. Graham, D. E. Knuth, and O. Patashnik, *Concrete Mathematics* (Addison-Wesley, Reading, Massachusetts, 1994), 2nd ed.
 - [44] S. B. Guthery, *A Motif of Mathematics* (Docent Press, Massachusetts, 2011).